Ti-Al-Si-C-N HARD COATINGS SYNTHESIZED BY HYBRID ARC ENHANCED MAGNETRON SPUTTERING[1]

Guizhi Wu [2]
Sitao Liu [2]
Shengli Ma [2]
Kewei Xu [2]
Vincent Ji [3]
Paul K Chu [4]

Abstract

Ti-Al-Si-C-N coatings are deposited by hybrid arc-enhanced magnetic sputtering and characterized by various micro- and macro-tools. X-ray diffraction, high-resolution transmission electron microscopy, and X-ray photoelectron spectroscopy reveal that the coatings are nanocomposites consisting of nanocrystallites and amorphous phases. They are generally in the form of nc-(Ti,Al)(C,N)/a-Si_3N_4/a-C depending on the composition of the coatings. With increasing Al concentrations, the X-ray diffraction peaks shift to a lower angle indicating compressive stress in the coatings. The measured hardness also diminishes implying reduced contributions from the self-organized stable nanostructure. The dry friction coefficients of the Ti-Al-Si-C-N coatings are found to be about 0.3 which is lower than that of conventional Ti-Si-N coatings. These coatings can find potential applications requiring high temperature with heavy contact loading.

Keywords: Ti-Al-Si-C-N coatings; Nanostructure; Hardness; Friction.

INTRODUCTION

New types of hard coatings with good potential applications in cutting tools, molds, etc. continue to attract attention,[1-3] although TiN and TiC coatings have been studied extensively and widely used in the industry since the early 1980s.[4] The reported results show that TiN coatings have high hardness of about 20 GPa[5,6] and in practice, TiN coated cutting tools and molds show better performance. TiC coatings have also been used successfully in industry.[7] However, TiN and TiC coatings cannot satisfy the more stringent requirements demanded by elevated temperature applications and consequently, new types of hard coatings have been studied. TiAlN hard coatings boasting a high hardness of over 30 GPa, good oxidation resistance in high temperature, and good wear resistance have been one of the most successful industrial coatings, especially in cutting applications.[8-10] It has been reported that TiAlN coatings have better wear resistance than TiN coatings, and the oxidation resistance of TiAlN coatings increases linearly with increasing aluminum contents.[11,12] TiSiN hard coatings have also been found to have superior properties. In 1995, the first publication concerning the design of novel superhard nanocomposites with hardness over 40 GPa was reported.[13] Studies of the microstructure of TiSiN coatings reveal a nanocomposite microstructure composed of a nanocrystalline phase of TiN surrounded by an amorphous phase of Si_3N_4. The super hardness is believed to arise from this nanocomposite microstructure.[14] However, the ever increasing demand by molds and high-speed cutting tools requires continuous improvement in the coating system and many new kinds of hard coatings have been produced.[15] However, based on our knowledge, there have been few reports on TiAlSiCN coatings. This paper reports the deposition of TiAlSiCN hard coatings with different Al concentrations by means of hybrid arc-enhanced magnetic sputtering. The deposition process and relationship between mechanical properties and microstructure are investigated in this work.

2 EXPERIMENTAL DETAILS

An arc-enhanced unbalanced magnetron sputtering hybrid sputtering (AEMS) system depicted schematically in Figure 1 was employed to deposit the Ti-Al-Si-C-N coatings. A titanium arc (arc target of Ti) was used to increase the plasma density due to arc discharge and to enhance adhesion between the coating and substrate. Three pairs of dual-magnetron targets including two Al targets, two C targets, and two Si targets were installed along the vacuum chamber wall. Two planar magnetrons of each pair were placed in the vacuum chamber. A rotatable substrate holder was placed in the center. A pulsed direct current (DC) power supply was used on the substrate and four pulsed alternating current (AC) power supplies of 40 kHz were used on each pair of dual-magnetron targets to control the substrate bias voltage, substrate bias current, and target power. The substrate bias power supply was operated in the unipolar pulse mode and the duty cycle (on-off) could be adjusted according to the process requirement. The medium-frequency power supplies used the current-constant mode to control the magnetron targets. Argon gas was introduced to each target to enhance sputtering of the targets. Before deposition, the polished high-speed steel (HSS) substrates were cleaned in an ultrasonic bath cleaner using acetone and ethanol. After pumping down to a background pressure of 6.0×10^{-3}Pa by a turbo-molecular pump, the substrate were further cleaned by Ar ion bombardment at a bias voltage of -1000 V and a duty ratio of 65% under an Ar

atmosphere of 6 Pa for 20 minutes in the vacuum chamber.
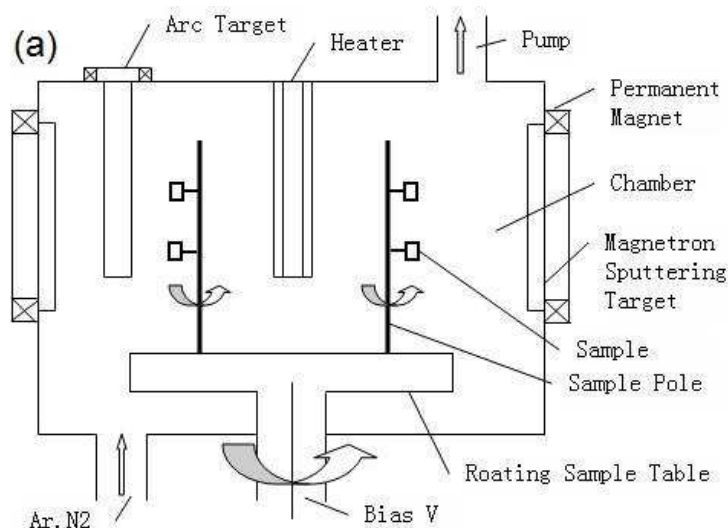
Figure 1. Schematic diagram of the arc-enhanced magnetron sputtering (AEMS) system.

The Ti-Al-Si-C-N coatings were synthesized at pulsed DC bias voltages of -100 V, substrate temperature of 200°C, and pressure of 0.3 Pa in a gas mixture of Ar (flow rate of 30 sccm) and N_2 (flow rate of 28 sccm). The power applied to the C target (6 kW) and Si target (3 kW) as well as the current at the Ti arc ion target (60 A) were kept constant and only the Al target power was varied from 3.5 to 30 kW. The substrate-to-target distance was 120 mm. In order to enhance the adhesion between the coating and substrate, a TiN interfacial layer with a thickness of about 100 nm was reactively sputtered onto the substrate from the Ti targets, and the deposited Ti-Al-Si-C-N coatings had a thickness of more than 3.0 μm.

The thickness and surface morphology of the coatings were measured using scanning electron microscopy (SEM, JSM 6700F). The composition of the coatings was determined by energy dispersive X-ray spectroscopy (EDS) by an Oxford INCA Energy detector installed on the JSM 6700F SEM. The chemical bond analysis was carried out by X-ray photoelectron spectroscopy (XPS, PHI 5802). The crystalline phase in the coating was performed by pseudo-glazing incidence X-ray diffraction (GIXRD) using Cu K_α radiation. A Shimadzu Limited Pro X-ray diffractometer was used to analyze the as deposited samples at an incident angle of 2°. The structural information was determined by high-resolution transmission electron microscopy (HR-TEM, JEM 2100F). The hardness values were determined employing an HV-100 microhardness tester equipped with a Vickers diamond indenter at an applied load of 200 mN in order that the depth of diamond indenter was below than 0.3 μm (less than 1/10 of the coating thickness). The measurement error in the HV-100 micro-hardness test was about 10%. The friction coefficients and wear behavior were evaluated by sliding tests using a pin-on-disk tribometer using a load of 3.25 N. A Si_3N_4 ball (3 mm diameter) was used as the counterpart. The sliding tests were conducted at a sliding speed of 0.3 m/s at 20°C and 45% relative humidity in air without applying lubricants. The binding force of coatings was evaluated by scratch tests using a WS-type scratch tester at a scratch speed of 60 N/min. The maximum load force was 100N. The residual stress values were determined by X-ray diffraction with the Panalytical X-pert system under Cu K_α radiation.

3 RESULTS AND DISCUSSION

Figure 2 shows the changes in the composition of the Ti-Al-Si-C-N coatings as a function of power applied to the Al target. The Al concentrations in the Ti-Al-Si-C-N coatings vary from 9 to 30 at% when the Al target power is changed from 2.5 to 15 kW. Meanwhile, the Ti concentrations change from 20 to 5 at%. The results suggest that Al atoms replace Ti atoms as the Al concentration increases. As shown in Figs. 3 and 5, we can conclude that Al atoms replace Ti atoms when the Al concentration increases. In comparison, the Si and C+N concentrations remain almost unchanged with the C+N concentration being almost constant at 57 at%. However, the C concentrations vary from 23 at% to 15 at% and N concentrations vary from 35 at% to 44 at% as the Al contents increase. Here, the C+N concentrations are used to make Fig. 2 easier to understand. The oxygen impurity concentration in the Ti-Al-Si-C-N coatings is less than 1 at%.
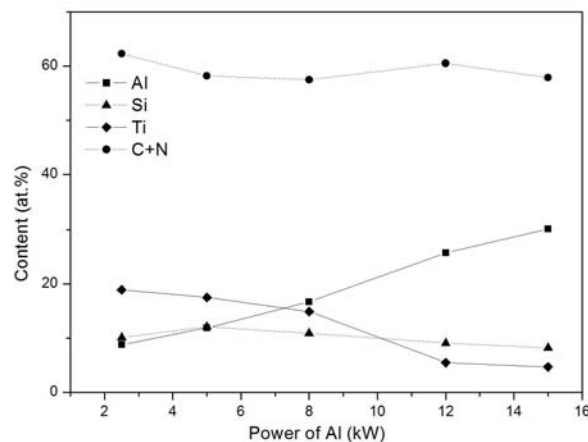
Figure 2. Compositional changes in the Ti-Al-Si-C-N coatings as a function of power applied to the Al target.

The GIXRD results acquired from the Ti-Al-Si-C-N coatings with different Al contents are displayed in Fig. 3. The dotted lines indicate the standard positions of fcc TiN (JCPDS 00-038-1420), fcc TiC (JCPDS 00-032-1383), fcc AlN (JCPDS 00-034-0679), and hex AlN (JCPDS 00-025-1133). The high peak at around 44⁰ in the 16 at% Al pattern is considered to be the substrate phase of HSS, which arises from the broken surface of this sample. The peaks at around 37° are found to shift significantly from their standard positions and all the phases exhibit broad peaks. The peaks are considered to be nanocrystalline (Ti,Al)(C,N). The peaks shift to a lower angle compared to the standard position with increasing Al concentrations. This indicates a larger lattice spacing in the phase compared to the standard phase or a phase change. As shown in Fig. 2, one reason may be replacement of Al atoms from TiN as the Al concentration increases. The phase changes from a high Ti content and low Al content (Ti,Al)(C,N) to a high Al content and low Ti content (Ti,Al)(C,N). As a result, the peaks shift to a lower angle compared to the standard position with increasing Al concentrations. Another possible explanation is the solid solution with larger Ti atoms in the AlN lattice causing lattice expansion and consequently, the peak shifts to a lower diffraction angle. More AlN lattices are formed as the Al concentration increases, so that more Ti atoms dissolve in the AlN lattices. This makes a lager lattice spacing in the phase and induces the peak shift. Further changes in the lattice spacing and subsequent peak shifts may be caused by residual compressive stress in the Ti-Al-Si-C-N coatings. The residual compressive

18th IFHTSE CONGRESS
International Federation for Heat Treatment and Surface Engineering
IFHTSE

ANAIS
PROCEEDINGS
ISSN 1516-392X

stress values of the Ti-Al-Si-C-N coatings decrease from 2500 MPa to 1700 MPa with increasing Al concentrations, as shown in Fig. 4. It indicates that adding Al can reduce the residual compressive stress in the Ti-Al-Si-C-N coatings. Other diffraction peaks from crystalline phases such as Si_3N_4 and C-C are not detected, indicating that Si and some C exist in the amorphous phase of silicon nitride and free C.
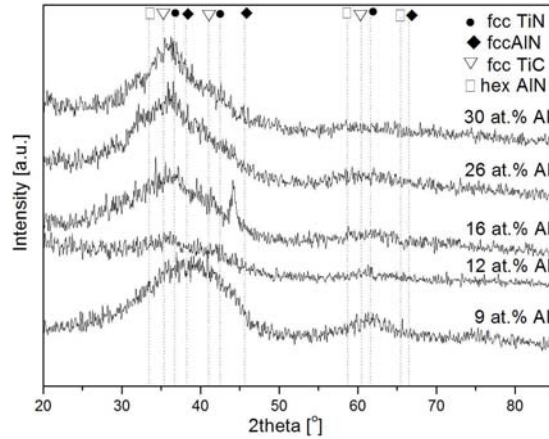
Figure 3. XRD investigations on as-deposited Ti-Al-Si-C-N coatings with different Al content.
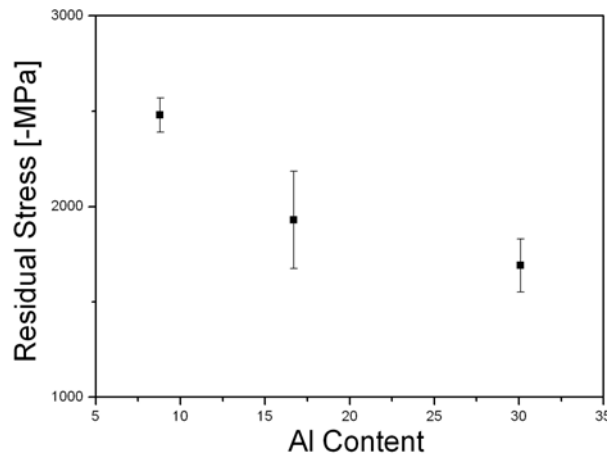
Figure 4. Residual compressive stresses of the Ti-Al-Si-C-N coatings with the increasing of Al content.

Figure 5 displays the TEM images of the Ti-Al-Si-C-N coatings with 9 at% (Fig. 5a) and 30 at% (Fig. 5b) Al. The SAED patterns on the right corner of Figures 5a and 5b indicate the existence of crystalline phases of (Ti, Al) (C, N) and the (Ti, Al) (C, N) crystallites have multiple orientations of (111), (200), (220).   The results are consistent with the X-ray diffraction patterns in Fig. 3.   The diffraction circles in Figs. 5a and 5b are continuous indicating small grain sizes. The Ti-Al-Si-C-N coating has a nanocomposite microstructure as shown in Figs. 5a and 5b, and the nanocrystallites (Ti, Al) (C, N) with a grain size of approximately 2 nm are embedded in the amorphous phase. This microstructure is believed to give rise to the higher hardness.
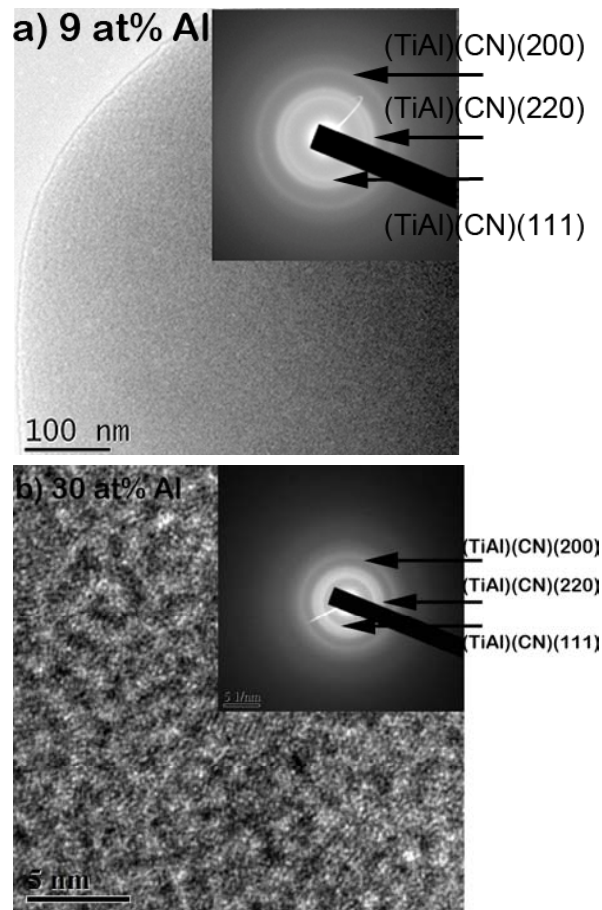
Figure 5. TEM images and SAED patterns of the Ti-Al-Si-C-N coatings with 9 at.% Al content(Fig. 5a) and 30 at.% Al content(Fig. 5b).

XPS is used to determine the bonding states in the Ti-Al-Si-C-N coatings. The spectra obtained from the Ti-Al-Si-C-N coatings with 9 at% Al and 26 at% Al are shown in Fig. 6 in which the Al 2p spectra show the Al-N peak at 73.8 eV. There is no evidence of the Al-C chemical bonding state in the coatings. The Ti 2p spectra in Figs. 6(b) and 6(B) show the Ti-C peak at 455.1 eV and Ti-N peak at 456.5 eV. It is consistent with the results in Fig. 3 and Fig. 5, indicating that the (Ti,Al)(C,N) crystalline phase exists in the Ti-Al-Si-C-N coatings. The C 1s spectra in Figs. 6(c) and 6(C) show the C-Ti peak at 282.5 eV, which is consist with the Ti 2p spectra. The C 1s spectra also show the C-C peak at 284.6 eV, demonstrating that some atoms exist as amorphous carbon (a-C) since no carbon crystalline phase is disclosed by Fig. 3 and Fig. 5. The Si 2p spectra in Figs. 6(d) and 6(D) show the Si-N peak at 101.7 eV indicating the existence of Si_3N_4. However, the XRD result in Fig. 3 and the TEM result in Fig. 5 do not disclose any crystalline Si_3N_4 phase, implying that Si_3N_4 should be in an amorphous form of a-Si_3N_4. Another peak of Si-O (100.6 eV) in Fig. 6(d) and Fig. 6(D), Al-O (75.7 eV) in Fig. 6(a) and Fig. 6(A), C-O (286.9) in Fig. 6(c) and Fig. 6(C) are perhaps due to oxygen contamination on the surface. Based on the results in Fig. 6, it can be inferred that C in the Ti-Al-Si-C-N coatings exists in the (Ti,Al)(C,N) crystalline phase and amorphous phase of C, whereas Si exists as a-Si_3N_4. Therefore, the Ti-Al-Si-C-N coating has a nanocomposite microstructure as shown in Fig. 3, Fig. 5 and Fig. 6, and the nanocrystallites (Ti,Al)(C,N) are embedded in the amorphous phase (a-Si_3N_4/a-C), so that the nanocomposite is nc-(Ti,Al)(C,N)/a-Si_3N_4/a-C. This microstructure is believed to give rise to the super high hardness.
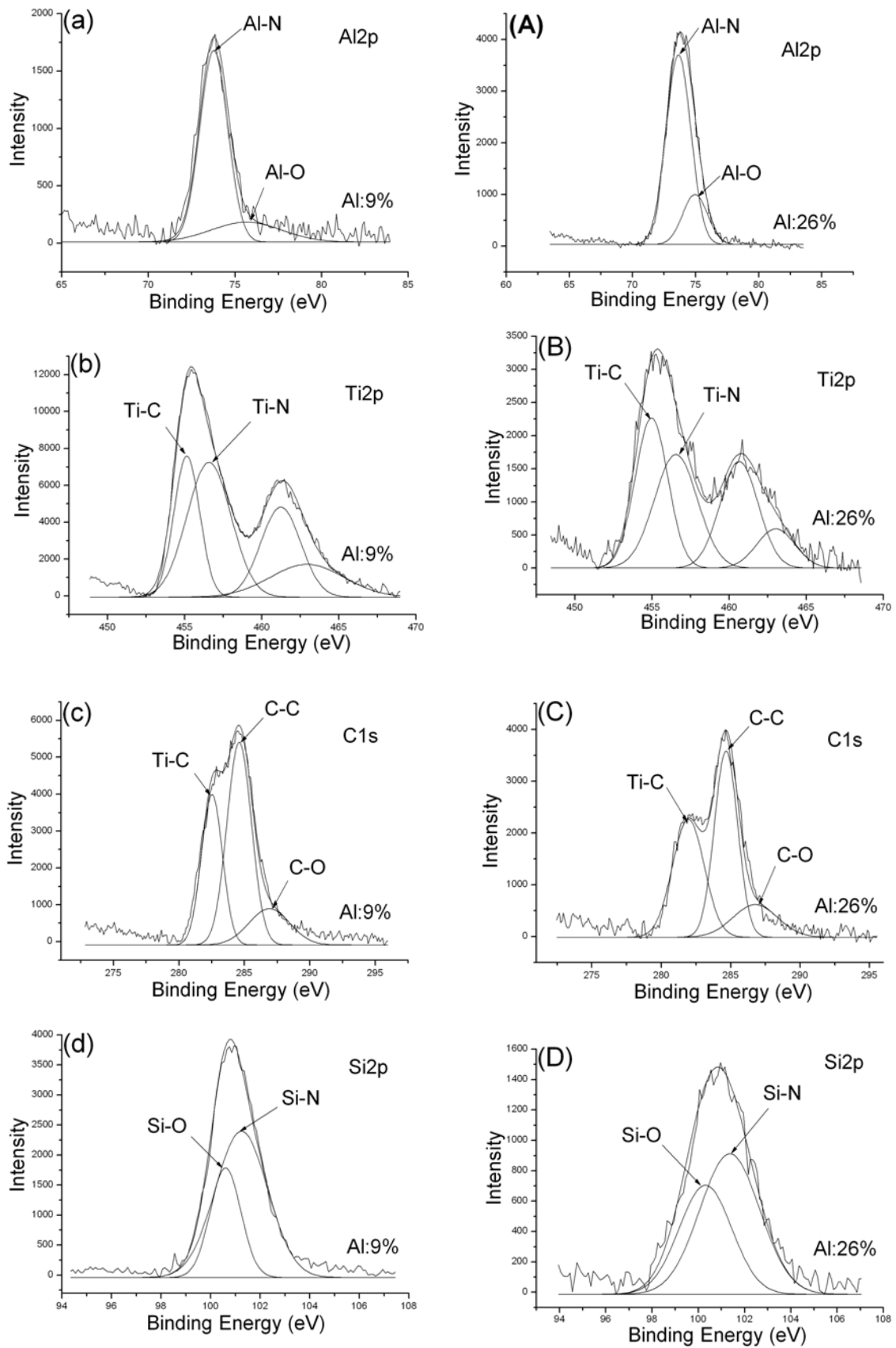
Figure 6. XPS spectras of the Ti-Al-Si-C-N coatings with 9 at.% Al content(Fig. 6a, 6b, 6c, 6d) and 26 at.% Al content(Fig. 6A, 6B, 6C, 6D).

Fig. 7 shows the hardness values determined from the Ti-Al-Si-C-N coatings containing various amounts of Al. The hardness values are obtained from samples having a thickness of more than 3.0 μm. As the Al content increases, the hardness increases and reaches the maximum value of approximately 38 GPa when the Al concentration is 12%. The Ti-Al-Si-C-N coatings possess a nanocomposite structure with (Ti,Al)(C,N) nanocrystallites embedded in a thin amorphous Si_3N_4/C matrix. This kind of structure limits cracks in the amorphous Si_3N_4/C matrix to several nanometers and impedes propagation of nano-cracks. It also reduces the movement of dislocations in the Ti-Al-Si-C-N coatings resulting in enhancement in the hardness. However, further increase in the Al concentration decreases the hardness of the Ti-Al-Si-C-N coating. The size of the nanocrystallite in the Ti-Al-Si-C-N coating increases when the Al content increases as shown in Fig. 3 and Fig. 5. The amorphous Si_3N_4/C matrix becomes thinner as the size of the crystallites increases. The thinner amorphous Si_3N_4/C matrix promotes propagation of nano-cracks thereby decreasing the hardness.
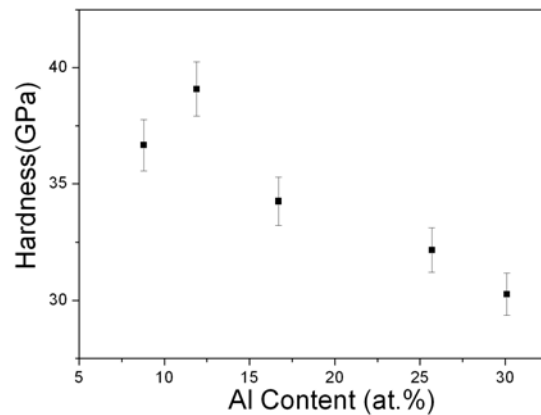
Figure 7. Hardness values of the Ti-Al-Si-C-N coatings with various Al contents.

Fig. 8 shows the binding force of the Ti-Al-Si-C-N coatings with various Al contents. At Al concentrations smaller than 26 at%, the binding force remains constant as the Al content varies. When the Al concentration increases to 30 at%, the binding force increases from 40 N to 50 N. The residual stress decreases as the Al content increases as shown in Fig. 4. Higher intrinsic residual stress makes it easier to destroy the coating. When the Al concentration increases, the residual stress decreases and the binding force increases. The micrographs showing the scratches are exhibited in Fig. 8 which shows that the coating peels off from the substrate when the coating-substrate system is destroyed.
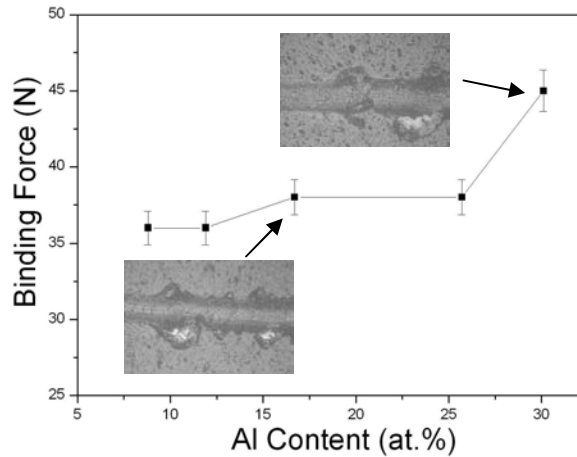
Figure 8. Binding force values and scratch images of the Ti-Al-Si-C-N coatings with various Al contents.

Fig. 9 displays the friction coefficients of the Ti-Al-Si-C-N coatings with various Al contents. The friction coefficients range from 0.3 to 0.45 at room temperature. For the samples with 9 at% and 12 at% Al, the friction coefficients are about 0.3. Meanwhile, the friction coefficients of the samples with 26 and 30 at% Al are about 0.45. The reason of the different friction coefficients should be the different C contents. The C concentrations in the samples with 9 at% and 12 at% Al are about 23 at%, but 15 at % in the samples with 26 at% and 30 at% Al. The low friction coefficients appear to be related to self-lubrication stemming from the formation of amorphous C acting as a graphite-like lubricating layer. It can be found that for the sample with 12 at% Al content, the friction coefficient is the lowest at 0.3, and the hardness is the highest at 38 GPa. This provides the foundation to fabricate Ti-Al-Si-C-N coatings with low friction coefficient and high hardness.
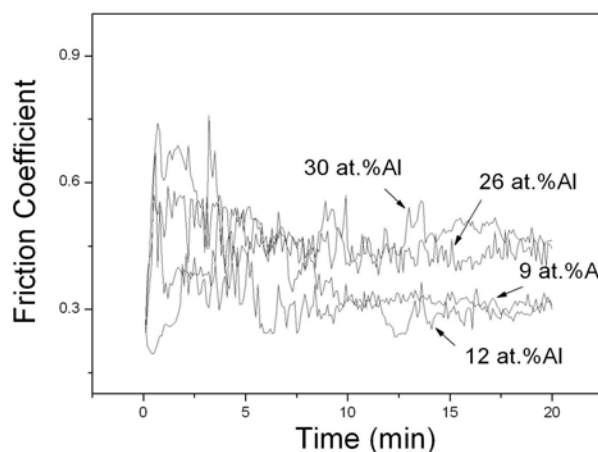
Figure 9. Friction coefficients of the Ti-Al-Si-C-N coatings with various Al contents.

4 CONCLUSION

Ti-Al-Si-C-N coatings with Al concentrations ranging from 9% to 30% were deposited by a hybrid arc-enhanced magnetic sputtering system. All coatings have a nanocomposite phase structure of nc-(Ti,Al)(C,N)/a-Si_3N_4/a-C.   The hardness of the Ti-Al-Si-C-N coatings reaches the maximum value of approximately 38 GPa when the Al concentration is 12%. The high hardness is believed to be due to the formation of

the nanocomposite microstructures. The lower friction coefficient of the Ti-Al-Si-C-N coatings is 0.3. On account of their high hardness and low friction coefficient, Ti-Al-Si-C-N coatings are potentially useful in dry and high-speed cutting tools.

Acknowledgements

REFERENCES

1   A.Vyas, Y.H.Lu, Y.G.Shen, Surf. Coat. Technol. 204(2010)1528-1534.
2   Yin-Yu Chang, Chi-Pang Chang, Surf. Coat. Technol. 204(2009)1030-1034.
3   S.Shimada, M.Takahashi, H.Kiyono, J.Tsujino, Thin Solid Films. 516(2008)6616-6621.
4   Xing-zhao Ding, A.L.K. Tan, X.T. Zeng, C. Wang, T. Yue, C.Q. Sun, Thin Solid Films. 516(2008)5716-5720.
5   T. S. Li, H. Li and F. Pan, Surf. Coat. Technol. 137(2001)225-229.
6   G. Abadias, S. Dub, R. Shmegera, Surf. Coat. Technol. 200(2006)6538-6543.
7   Y.T. Pei, D. Galvan, J.Th.M. De Hosson, A. Cavaleiro, Surf. Coat. Technol. 198(2005)44-50.
8   S. PalDey, S.C. Deevi, Mater. Sci. Eng. A342 (2003) 58.
9   G.S. Fox-Rabinovich, G.C. Weatherly, A.I. Dodonov, A.I. Kovalev, L.S. Shuster, S.C. Veldhuis, G.K. Dosbaeva, D.L. Wainstein, M.S. Migranov, Surf. Coat. Technol. 177-178 (2004) 800–811.
10 W. Grzesik, Z. Zalisz, S. Krol, P. Nieslony. Wear. 261 (2006) 1191-1200.
11 J.C. Oliveira, A. Manaia, A. Cavaleiro, Thin Solid Films. 516(2008)5032-5038.
12 Chung Wan Kim, Kwang Ho Kim, Thin Solid Films. 307(1997)113-119.
13 S. Veprek, S. Reiprich, L. Shizhi, Appl. Phys. Lett. 66(1995)2640.
14 S. Veprek, A. Niederhofer, K. Moto, T. Bolom, H.D. Mannling, P. Nesladek, Surf. Coat. Technol. 133-134(2000)152-159.
15 S.L. Ma, D.Y. Ma, Y. Guo, B. Xu, G.Z. Wu, K.W. Xu, Paul K. Chu. Acta Materialia. 55 (2007) 6350-6355.